Deep–Sea Research I 195 (2023) 104005

Contents lists available at ScienceDirect

Deep-Sea Research Part I

journal homepage: www.elsevier.com/locate/dsri

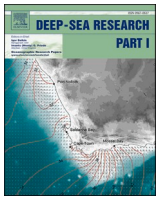

Estimation of nitrate concentration and its distribution in the northwestern Pacific Ocean by a deep neural network model

Lixin Wang [a,b], Zhenhua Xu [b,c,d,e,f,*], Xiang Gong [a,**], Peiwen Zhang [b,c,d], Zhanjiu Hao [b,c,d,e], Jia You [b,c,d,e], Xianzhi Zhao [a], Xinyu Guo [g]

[a] School of Mathematics and Physics, Qingdao University of Science and Technology, Qingdao, China
[b] CAS Key Laboratory of Ocean Circulation and Waves, Institute of Oceanology, Chinese Academy of Sciences, Qingdao, China
[c] Pilot National Laboratory for Marine Science and Technology, Qingdao, China
[d] Center for Ocean Mega-Science, Chinese Academy of Sciences, Qingdao, China
[e] College of Earth and Planetary Sciences, University of Chinese Academy of Sciences, Beijing, China
[f] CAS Engineering Laboratory for Marine Ranching, Institute of Oceanology, Chinese Academy of Sciences, Qingdao, China
[g] Center for Marine Environmental Study, Ehime University, 2-5 Bunkyo-cho, Matsuyama, 790-8577, Japan

ARTICLE INFO

Keywords:
Nitrate
Spatial distribution
Deep neural network
Northwestern pacific ocean

ABSTRACT

As a fundamental nutrient for marine biogeochemical processes, the magnitude and spatial distribution of nitrate concentrations are insufficiently measured in the interior ocean. In the present study, a deep neural network (DNN) model was developed to estimate nitrate concentrations in the upper northwestern Pacific Ocean (NPO). This model takes the temperature and salinity profiles as the primary input variables. Since the subtropical and tropical regions are featured by different spatial patterns of nitrate concentrations, we separately trained the model to improve the prediction skill. The predictive results indicate that the DNN model performs well in depicting both spatial and seasonal variability of nitrate concentrations. The sensitivity experiments show that temperature is the dominant factor for the nitrate estimation, while salinity has a relatively small effect, but it cannot be ignored in improving the prediction accuracy. Furthermore, using the temperature and salinity data from World Ocean atlas (2018), we found our DNN model has a good generalization ability on nitrate estimation in NPO. This model can be applied to further studies on nitrate's spatiotemporal variability and mechanism around the global ocean.

1. Introduction

As a principal nitrogenous substance, the nitrate plays a key role in nutrient support for the photosynthesis in the ocean through the direct consumption by the primary producers. The spatial distribution and temporal variability of the nitrate are heterogeneous due to the consumption of biogeochemical processes (Webb, 2021). The northwestern Pacific Ocean (NPO), an essential transportation channel for nitrate and other nutrients, is very critical for the global biogeochemical fluxes (Sarmiento et al., 2004; Tsunogai, 2002). In the past century, the nitrate in the NPO has increased rapidly (Kim et al., 2011). Given the possible impact of rapid nitrate changes in the NPO on ecological environment conditions (Li and Wang, 2013), it is of significance to strengthen the observation ability of marine nitrate concentration and develop methods to estimate nitrate concentration (Wang et al., 2018).

The spatial distribution of nitrate, especially the vertical profile, is the key to reveal the uptake and replenishment of nitrate (Kanda, 2008). The in-situ observations and Biogeochemistry Argo (BGC-Argo) are the commonly used methods to measure nitrate concentrations (Talley et al., 2016; Yang et al., 2020). However, the high cost leads to the coarse and insufficient spatiotemporal sample resolution. The in-situ observation cannot accurately record the continuous change of nitrate, which further limits the understanding of biogeochemical processes (Sauzède et al., 2017). In addition to the direct observation, previous studies use various properties, including temperature, salinity, chlorophyll, etc., to empirically estimate nitrate concentration (Goes et al., 2000; Guo et al., 2014; Huang et al., 2016; Xiu and Chai, 2011; Yasunaka et al., 2014; Zhou et al., 2021). However, the empirical formula has a

* Corresponding author. CAS Key Laboratory of Ocean Circulation and Waves, Institute of Oceanology, Chinese Academy of Sciences, Qingdao, China.
** Corresponding author.
E-mail addresses: xuzhenhua@qdio.ac.cn (Z. Xu), gongxiang@qust.edu.cn (X. Gong).

https://doi.org/10.1016/j.dsr.2023.104005
Received 30 November 2022; Received in revised form 20 February 2023; Accepted 21 February 2023
Available online 23 February 2023

poor performance on the estimation of nitrate concentration due to the complex relationships between nitrate and other properties.

Machine learning is a promising tool for solving this problem since it can fit the nonlinear relationship between multiple parameters (Dong et al., 2022; X. Li et al., 2022; Z. Li et al., 2022; Zhang and Li, 2022). Many kinds of neural networks have been utilized in the geophysical and biogeochemical community over the past few decades (Friedrich and Oschlies, 2009; Jamet et al., 2012; Mustapha et al., 2014). In early days, the artificial neural network (ANN) has been applied to construct a model to estimate nutrient concentrations (Sarangi, 2011; Zare et al., 2011). Steinhoff et al. (2010) used a self-organizing map for estimating two-dimensional sea surface nitrate in the North Atlantic and North Pacific. However, the ANN model has only one hidden layer, which easily falls into the problem of local minima and overfitting and results in an inaccurate estimation. DNN with more hidden layers can overcome the drawbacks of ANN (Khumprom and Yodo, 2019; Kim et al., 2019). In addition, the drop-out method in the DNN model can handle unexpected outliers efficiently. Therefore, the DNN model has recently been widely used to estimate nitrate concentration in the world's oceans (Fourrier et al., 2020; Sauzède et al., 2017).

As a data-driven method, a large amount of observation is needed to build a DNN model. Benefiting from the seasonally repeated cruises by the Japan Maritime Agency (JMA) in the NPO, many observed profiles of nitrate were obtained. Therefore, it can be used to build and train the DNN model. Because of the importance of nitrate transport in NPO, the studies on the spatial distribution of nitrate have never stopped (Goes et al., 1999; Rafter et al., 2012; Yasunaka et al., 2014). To map the spatial distributions of nitrate concentration in upper 1000 m of NPO, we developed a regional model based on the DNN structure. The different ocean environments, including the circulation system, stratification, internal wave field, etc., feature the subtropical and tropical regions with distinct characteristics (Chen et al., 2021; Feng et al., 2010; Sun et al., 2007). The relationship between nitrate and other variables may be affected by the above factors. Because the DNN model is data dependent, inconsistent relationships between input and output variables in different regions will affect results. Hence, we separately built the DNN model in subregions, including the subtropical region and the tropical region, which can have better performance on estimating (Chen et al., 2022; Goes et al., 1999). Based on the data from World Ocean Atlas (2018) (WOA18), we further assessed the generalization ability of our DNN model on nitrate estimation in NPO.

The remainder of the paper is organized as follows: Section 2 describes the details of the data, model and evaluation methods used in this study. Section 3 demonstrate the performance of the DNN model. The sensitivity of input variables of the model and the spatial distribution of nitrate are discussed in Section 4. Section 5 is the summary.

2. Data and methods

2.1. Data

The in-situ data used in the model are measured by the Japan Meteorological Agency (JMA) from January 2015 to March 2021 (https://www.data.jma.go.jp/). The observations were carried out by R/V *Keifu* and R/V *Ryofu* at 120°E–180°E and 9°S–34°N. Quality control is necessary before collating these observations into a dataset used for the DNN model. There are two criteria for quality control: (1). the profiles whose depths are less than 1000 m are not considered; (2). the profile whose missing values account for more than half of the total data are excluded. Then we applied linear interpolation on these pre-processed data to fill in the missing values (Chen et al., 2022; Sammartino et al., 2018). After pre-processing, a dataset including 832 vertical nitrate profiles covering January 2015 to March 2021 was used to train and test the designed DNN model (Fig. 1).

WOA18 (Garcia et al., 2019) was also used to evaluate the generalization ability of the DNN model. This monthly dataset can be downloaded from the Asia Pacific Data Research Center (ARDRC, http://apdrc.soest.hawaii.edu/as/v6/search), with a spatial resolution of 0.25° × 0.25°. Temperature and salinity from WOA18 were standardized before input to make them dimensionless and of the same order of magnitude. For each grid, all data are clustered around 0 with a variance of 1.

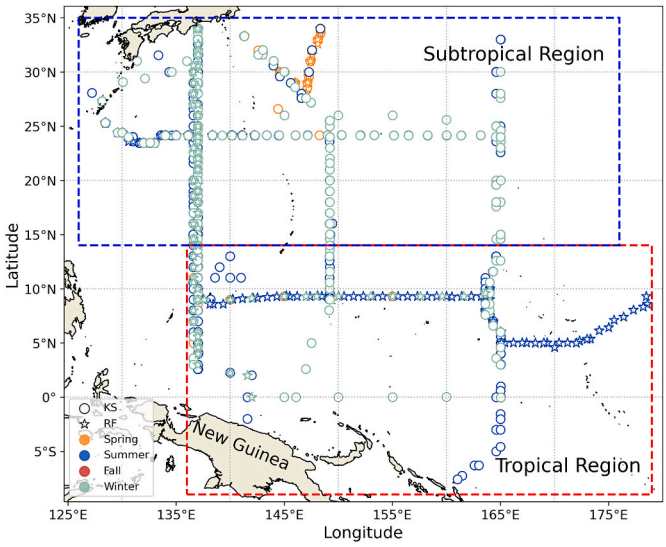

Fig. 1. Geographic distribution of 832 vertical profiles from the dataset of Japan Meteorological Agency (JMA) in the northwestern Pacific Ocean (NPO) used in this study. Different shapes of symbols represent R\V *Keifu* (KS) and R\V *Ryofu* (RF), respectively. The season are marked with different four colors.

2.2. DNN model

The DNN model is a more sophisticated artificial neural network with multiple hidden layers. The connection of multiple hidden layers enables the model to fit complex relationship between the input variables (i.e., temperature, salinity, location, time, etc.) and the output variables (i.e., Nitrate concentration). As shown in Fig. 2, DNN generally includes the input layer, several hidden layers and output layer. The DNN model transmits signals from the input layer to the hidden layers through forward propagation. The processed signals from the neurons in hidden layers are further transmitted into the output layer and then output an initial value. After the comparison between the initial value and the target value, backward propagation is used to adjust the weight of signals in the hidden layers and further reduce the error using the optimization algorithm. The activation function is added in the hidden layers to improve the fitting ability of the model. Compared to Sigmoid and Tanh activation function, ReLU does not use all neurons to avoid overfitting during the training process (Lu et al., 2020). At the same time, because the derivative of ReLU function is constant, the training process will not suffer from the problem of gradient disappearance, so that a deeper network structure can be available. The SoftMax function is adopted to prevent from the value of gradient becoming zero, since the weights and biases are not updated in every backpropagation step during the training process (Sharma et al., 2017). Therefore, in the front and rear hidden layers, the activation function is ReLu, and the activation function in the middle hidden layer is SoftMax.

2.3. Training process

The input variables used in the training process are latitude, longitude, temperature, salinity, time (month), and depth (Fig. 2). The reason for choosing geolocation and observation time is that the nitrate distribution varied seasonally and spatially. The model can find the

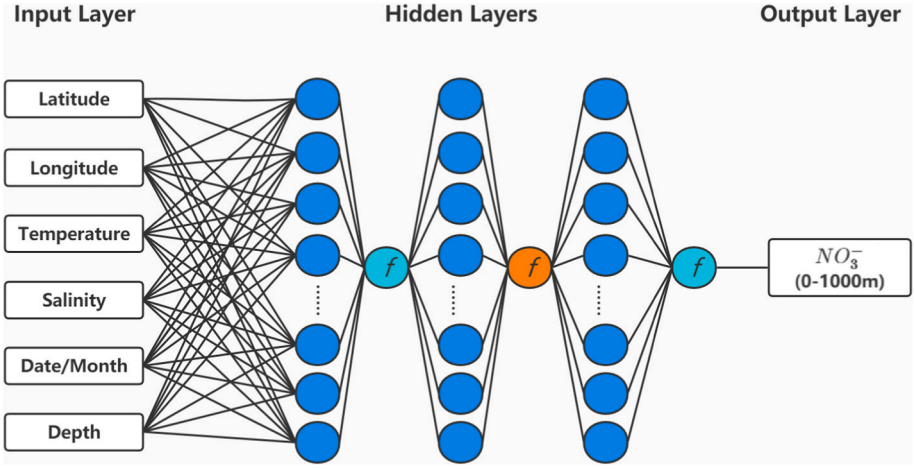

Fig. 2. The schematic representation of the deep neural network (DNN) model. *f* is the activation function, including ReLu (cyan) and SoftMax (orange).

nonlinear relationship between the input variables and the nitrate concentration at different depths (Bittig et al., 2018; Sauzède et al., 2017; Steinhoff et al., 2010). The output is the vertical distribution of nitrate concentration from sea surface to 1000 m.

The DNN model was trained by 80% of the profiles, and tested by the remaining 20% in each region. To efficiently update the network weights and accelerate convergence, the Adam optimizer is used with optimizer learning rate of 0.01 to reduce the loss in the training process. In addition, to avoid over-fitting, we applied the dropout technique to discard some neurons. During the training process, 15% of the training set was randomly selected as a validation set to verify whether the DNN model was over-fitted. The mean square error (MSE) of the training set and the verification set is taken as a loss function:

$$MSE = \frac{1}{n}\sum_{i=1}^{n}\left(x_i^{obs} - x_i^{pre}\right)^2 \quad (1)$$

According to the performance of the training set and validation set, the parameters of the DNN model were determined for each region (Table 1).

2.4. Statistical evaluation index

Three statistical indexes were chosen: the mean absolute error (MAE), the root mean squared error (RMSE), and the Nash-Sutcliffe efficiency criteria (NSE). The MAE and RMSE are commonly used to evaluate the error of the machine learning model, the NSE is commonly used to quantify the simulation accuracy (Lou et al., 2021; Sun et al., 2021; Uddin et al., 2022).

$$MAE = \frac{1}{n}\sum_{i=1}^{n}\left|x_i^{obs} - x_i^{pre}\right| \quad (2)$$

Table 1
Model parameters.

Model parameter	Parameter setting	
	Tropical region	Subtropical region
Hidden layer depth	3	3
Numbers of neurons per hidden layer	64,64,64	64,64,64
Learning rate	0.01	0.01
Dropout rate	0.05	0.05
Batch size	60000	60000
Epoch	150	150
optimizer	Adma	Adma
Training set	80%	80%
Validation set	15% of training set	15% of training set
Test set	20%	20%

$$RMSE = \sqrt{\frac{1}{n}\sum_{i=1}^{n}\left(x_i^{obs} - x_i^{pre}\right)^2} \quad (3)$$

$$NSE = 1 - \frac{\sum_{i=1}^{n}\left(x_i^{obs} - x_i^{pre}\right)^2}{\sum_{i=1}^{n}\left(x_i^{obs} - x_{mean}^{obs}\right)^2} \quad (4)$$

3. Results

3.1. The regional performance of DNN model

Before assessing the regional performance of the DNN model, we check the impact of the data amounts on the model performance. It is found that both the RMSE and MAE converge after the percentage of data used reaching 60% of total 832 profiles (figure not shown). The regional performance of the trained DNN model in the tropical and subtropical regions has been evaluated using the test dataset. Similar with the training process, the data on the test set is normalized in the same way. The model output is back-normalized to compare with the original data and measure model's performance.

Scatter plots of nitrate concentrations from the JMA observations and the model estimates show that most of the points are close to the diagonal bisector, while only very few data points diverge from it, with a low RMSE value of 0.7 μmol/L and a high NSE values of 0.99 (Fig. 3). These results suggest that the nitrate concentration estimated by the model is close to the observed value. It means our model performs well in the magnitude of nitrate concentration for the upper 1000 m in both tropical and subtropical regions.

Compared with the observed profiles of nitrate concentration in each region, the model estimates are very close to the observed results in both values and vertical structures (Fig. 4). The mean value of nitrate estimates from the DNN model almost coincides with that of the observations, and their biases are also small (Fig. 4c and f). The model performance in the tropical region is slightly worse than that in the subtropical region, especially in depth with high nitrate gradient (Fig. 4c). In the tropical region of NPO, the cyclonic circulation pattern causes the seawater's divergence and upwelling, resulting in shallower thermocline and promoting the upward supply of nutrients (Lukas and Lindstrom, 1991; Ma and Sun, 2015). By contrast, in the subtropical region, the anticyclonic circulation pattern makes the seawater converge and sink, leading to deeper thermocline which impedes the upward supply of nutrients from the deeper layers (Long et al., 2022; Ren and Riser, 2010). Because of the reverse T-N relation, the vertical profiles of nitrate are similar to the temperature profiles (Figs. 4 and 5, Goes et al., 2000; Morin et al., 1993; Kudela and Dugdale, 1996).

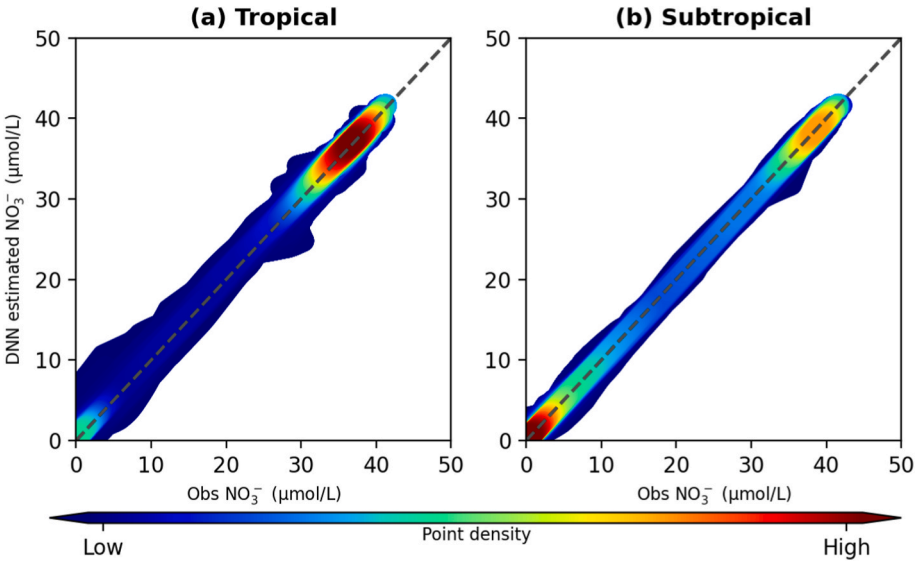

Fig. 3. Scatter plots of the observed nitrate concentration (x-axis) and the estimated nitrate concentration (y-axis) based on the test datasets of the (a) tropical region and (b) subtropical region. The black dotted line is the diagonal bisector, and the color indicates the point density.

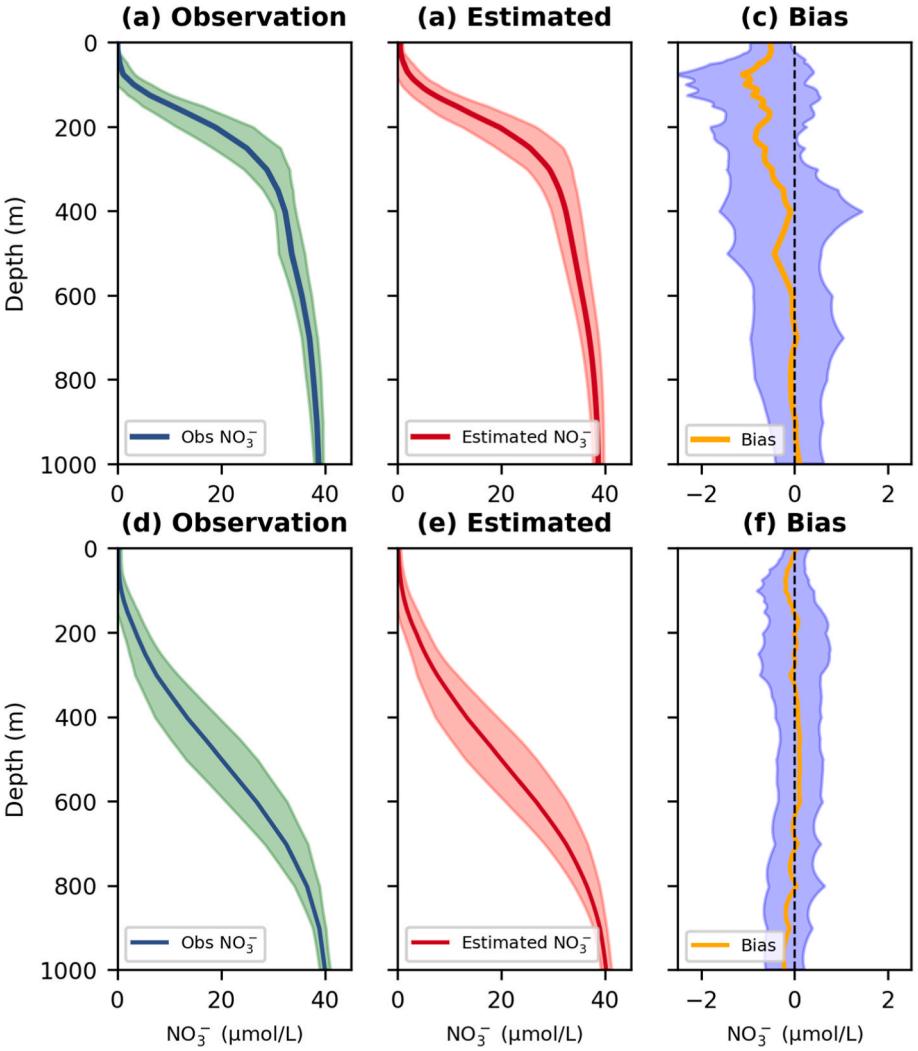

Fig. 4. Vertical profiles of (a) the observed nitrate concentration, (b) the model estimates and (c) the bias between observation and model estimates in the tropical region. The color shadings are the standard variances. (d–f) Same as (a–c) but in the subtropical regions.

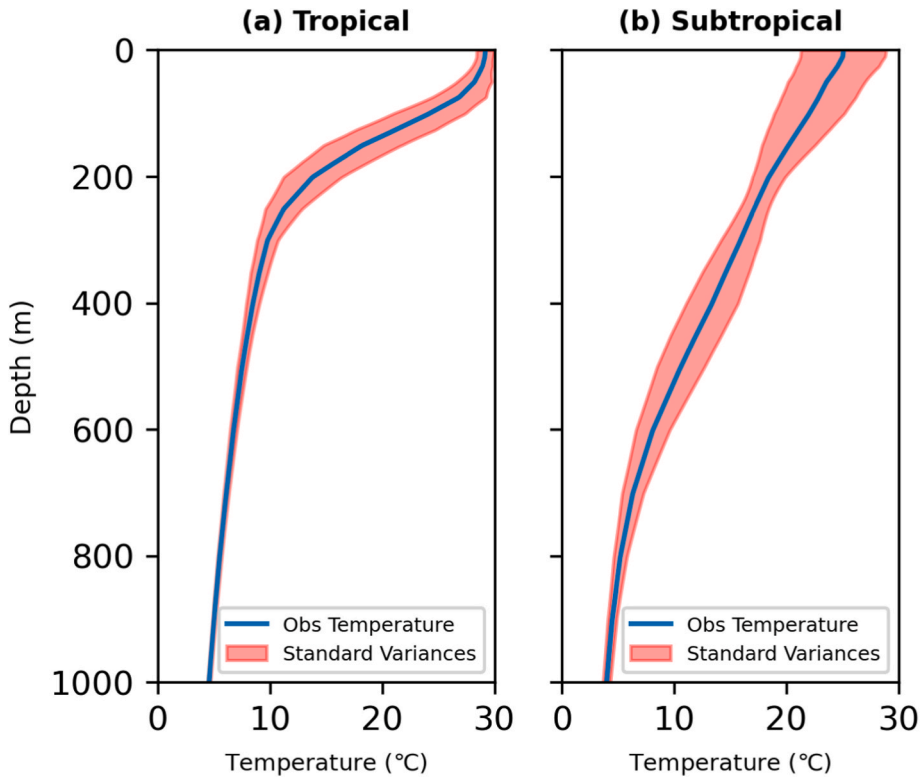

Fig. 5. Vertical profiles of the observed temperature in the (a) tropical region and (b) subtropical region. The pink shading is the standard variances.

Resulting in different model effects in the two areas. Both the nitracline and thermocline occur in 50–300 m of tropical region, and the model's performance in this area is relatively poor. Overall, the performance of the DNN model in tropical region and subtropical region is satisfactory.

We evaluate the performance of the DNN model according to three key statistical parameters (Table 2). High NSE values are shown in both regions, which suggests that input variables can explain over 99% of nitrate variability at different depths (Sauzède et al., 2017). The RMSE value is 0.92 μmol/L (0.48 μmol/L) and the MAE value is 0.72 μmol/L (0.38 μmol/L) in the tropical (subtropical) regions. It means the magnitudes of nitrate concentration in both two regions are well estimated. As shown in Fig. 4 c and f, the mean bias error show that maximal bias (0.5–1.1 μmol/L) occurs at about 40–300 m in the tropical region, while in the subtropical region, the large mean bias error merge about 40–180 m. This difference illustrates that our subregion-based model depicts different features of the nitrate profiles over the two regions and that the model performs well in predicting the vertical structure.

3.2. The seasonal performance of DNN model

To assess the model's capability to estimate nitrate in different seasons, the vertical profiles of estimated nitrate in summer (June to August) and winter (December to February) are shown in Fig. 6 and Fig. 7. The regionally averaged nitrate profile predicted by the DNN model is comparable to the observations in both two seasons. The predicted nitrate concentrations fluctuate within the observation variances with small biases. In the tropical region, nitrate concentration estimated by the DNN model has a slightly higher bias in winter, compared to summer (Fig. 6a–f), which is similar the research results of Silió-Calzada et al. (2008). The upper thermocline undergoes a seasonal vertical migration in the tropical region: shallower in summer and deeper in winter (Yu and McPhaden, 1999). Because the undulations in the nitracline followed that of the thermocline, the seasonal variations of nitrate profiles are similar to that of temperature profile (George et al., 2013). In the subtropical region, the average values almost coincide, and the standard variances are comparable (Fig. 7a–f). Although the seasonal variation in the thermocline is more significant in the subtropical region, almost all the nitrate in the upper layer is depleted, resulting in less seasonal variation in nitrate (Yasunaka et al., 2014). Unlike the results in the tropical region, the vertical profile of bias is so close to the zero line. In general, the model performs better in the subtropical region than in the tropical region. The difference in the performance may be due to the different nitrate change rate in the two regions (Lewis et al., 1986; Rafter et al., 2012).

Table 2
Statistical parameters of the DNN model in the tropical and subtropical regions.

Evaluation indicators	Tropical region	Subtropical region
NSE	0.99	0.99
RMSE (μmol/L)	0.92	0.48
MAE (μmol/L)	0.72	0.38

3.3. The zonal and meridional performance of DNN model

To further verify the prediction ability of the DNN model, two key observed sections were selected: one is the zonal section along 9°N from 136°E to 164°E, and the other is the meridional section along 137°E from 13°N to 35°N. Fig. 8 shows the vertical distribution of nitrate concentrations along the 9°N section and 137°E section from JMA data and the DNN model estimations. It can be clearly seen that the spatial distribution of the model estimated nitrate agrees well with the JMA observations. Most of the observed features are well reproduced by the DNN model.

For the 9°N section, the nitrate concentration changes significantly with depth in the upper 200 m. Below 200 m, the nitrate concentration rises from 30 μmol/L at 200 m to 40 μmol/L at 1000 m, and the vertical gradient getting decreases as depth increases (Fig. 8a and b). The nitrate concentration below 200 m estimated by the model is slightly smaller than the JMA observation, with the differences (JMA minus DNN) up to

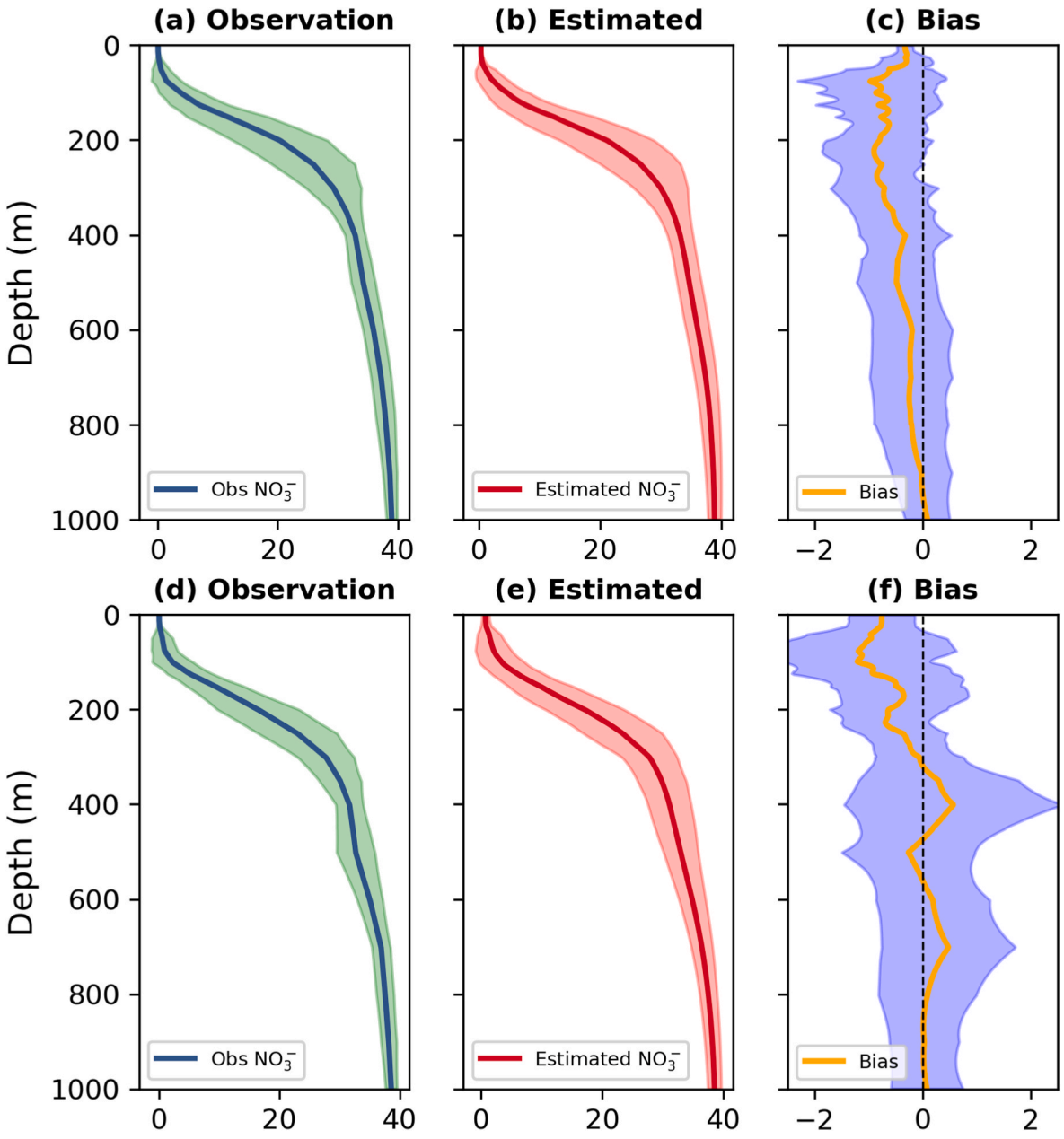

Fig. 6. Vertical profiles of (a) the observed nitrate concentration, (b) the model estimates, and (c) the bias between observation and model estimates in the tropical region during summer. The color shadings are the standard variances. (d–f) Same as (a–c) but during winter.

1.5 μmol/L (Fig. 8c). The most obvious difference occurs within the 100–200 m depth, where the estimated nitrate is relatively larger than the JMA observations with a maximum difference of more than 2 μmol/L. It should be noted that the 100–200 m depth corresponds to the thermocline. The changing temperature in the thermocline may affect the performance of the DNN model.

For the 137°E section, as shown in Fig. 8f, relatively large nitrate differences are present in the depth range of 100–150 m between 17.5°N and 22.5°N, and the JMA values are 2 μmol/L higher than the estimated values. The subtropical front in the Subtropical Countercurrent region cause rapid change of temperature and salinity in this area, thus reducing the accuracy of the model (Zhang et al., 2007). The errors in the DNN model along the 9°N section and 137°E section are about 0.43 μmol/L and 0.32 μmol/L, respectively. The results show that the DNN model can well depict nitrate concertation's zonal and meridional variations.

3.4. Performance comparison between DNN and ANN model

Prior to this study, the ANN model has been commonly applied to estimate nitrate concentration (Wang et al., 2018; Zhang et al., 2002). Compared with the DNN model, the ANN model has only one hidden layer. To evaluate the improvement of model performance by including more hidden layers, we used the same datasets to train and test both the ANN and DNN model.

As shown in Table 3, both the RMSE and MAE of DNN model are lower than that of ANN. The RMSE of DNN model in the tropical region is 0.25 μmol/L less than 0.17 μmol/L of the ANN model, and model error is reduced by about 21%. In the subtropical region, the RMSE of the DNN model is 14% smaller than that of the ANN model. Compared with the ANN model, the DNN model with more hidden layers can significantly reduce the estimation error of nitrate concentration.

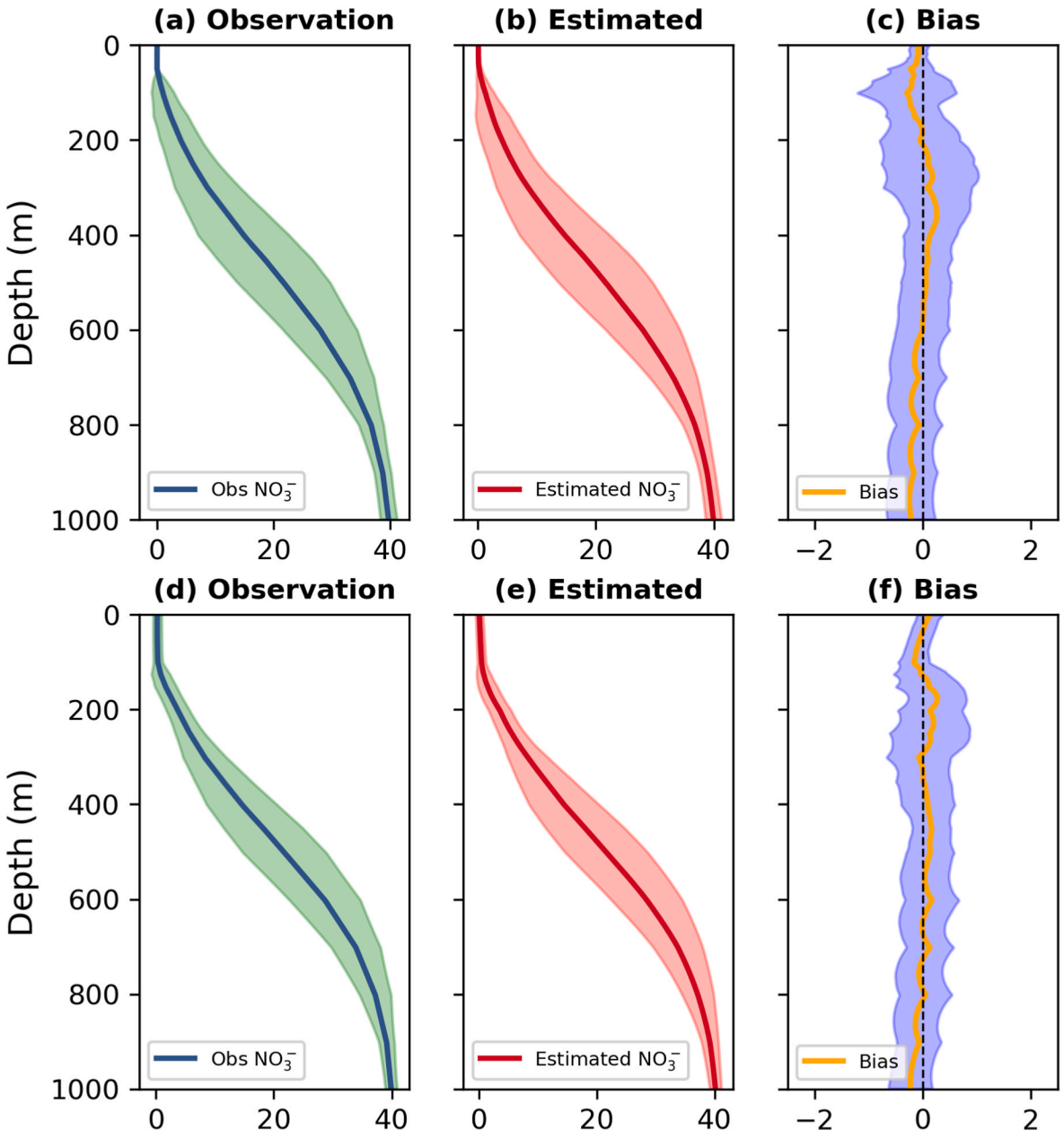

Fig. 7. Vertical profiles of (a) the observed nitrate concentration, (b) the model estimates, and (c) the bias between observation and model estimates in the subtropical region during summer. The color shadings are the standard variances. (d–f) Same as (a–c) but during winter.

4. Discussion

4.1. Sensitivity of input variables

Through forward and backward propagation, the DNN model adjusts the weight of input variables and extracts the implicit relationship for model estimation (Reichstein et al., 2019). However, different input variables will greatly affect the prediction skill of the model (Gevrey et al., 2003; May et al., 2011). Traditional methods for estimating nitrate concentration mostly only consider temperature, because there is an apparent relationship between temperature and nitrate (Kudela and Dugdale, 1996; Morin et al., 1993). However, the complex spatial and temporal variability of the temperature-nitrate relationship hinders its further application in large regions (Sun et al., 2007; Silió-Calzada et al., 2008).

Our designed model not only considers temperature, but also the salinity, whose impact on the estimation should not be ignored (Garside and Garside, 1995). To investigate how salinity affect the accuracy of estimation, a series of sensitivity experiments were set up (Table 4). In the Experiment 1, salinity is not considered as the input variable, while in Experiment 2, the salinity is included. In the tropical region, the RMSE of the estimated nitrate in the Experiment 1 is 1.01 μmol/L, and the MAE is 0.73 μmol/L. While the RMSE and MAE of estimated nitrate in the Experiment 2 are 0.92 μ mol/L and 0.72 μmol/L, respectively. In the subtropical region, the RMSE and MAE of Experiment 1 are 0.58 μmol/L and 0.46 μmol/L, while the RMSE and MAE of Experiment 2 are decreased obviously and are 0.48 μmol/L and 0.38 μmol/L, respectively. In subtropical region, inputting salinity can significantly increase the performance of the DNN model with a decrease of ~17% in RMSE and MAE. It means that the estimation from the DNN model fits the observations better when considering salinity. The improvement is not evident in the tropical region, where the RMSE and MAE decreased by only 9% and 1.4%, respectively. The results suggest that salinity can make the nitrate estimation more accurate, especially in high latitudes.

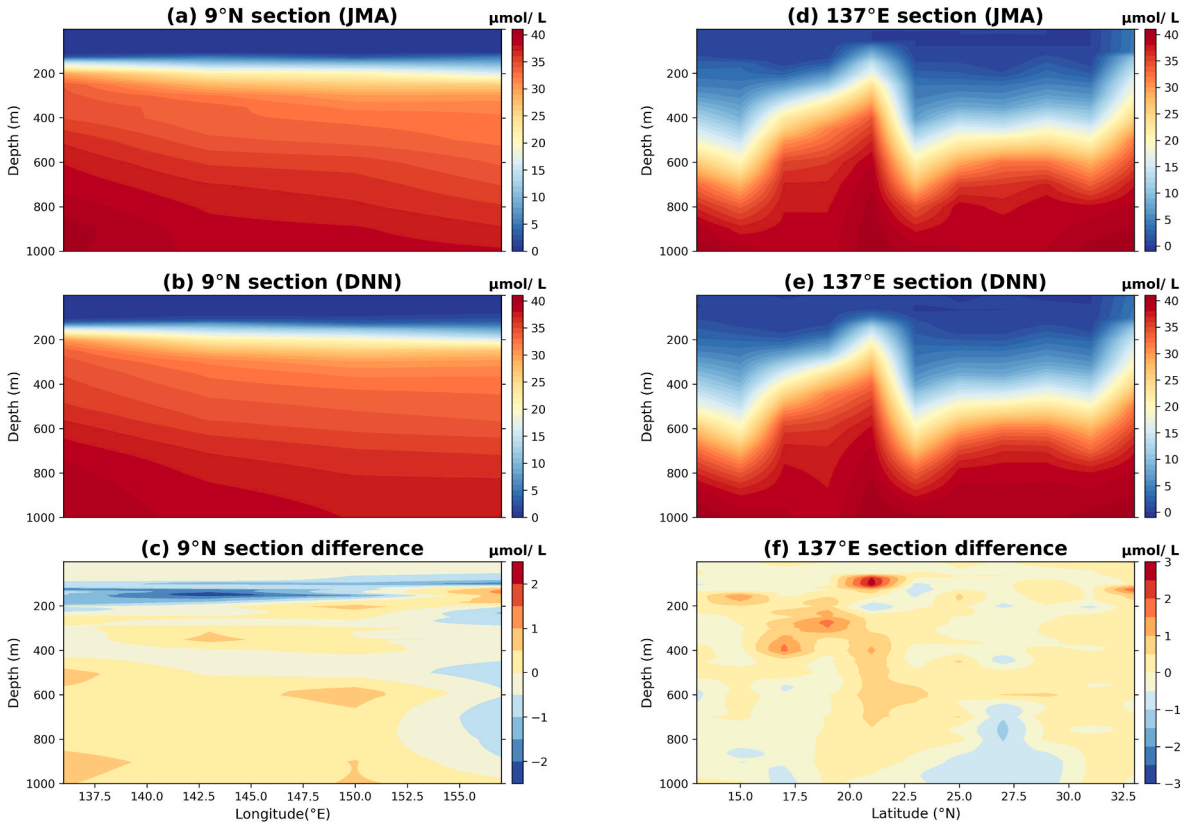

Fig. 8. Vertical distribution of nitrate concentrations along the 9°N section derived from (a) observation data and (b) the model estimates. (c) The difference between (a) and (b). (d–f) Same as (a–c) but along the 137°E section.

Table 3
Performance indicators of the ANN and DNN model based on the 20% validation dataset.

Study area	Evaluation indicators	Model	
		ANN	DNN
Tropical region	RMSE (μmol/L)	1.17	0.92
	MAE (μmol/L)	0.94	0.72
Subtropical region	RMSE (μmol/L)	0.57	0.49
	MAE (μmol/L)	0.46	0.38

Table 4
Performance indicators of the DNN model in the sensitivity experiments.

Experiments	Study area	Evaluation indicators	DNN	Improvement
Experiment 1 (without salinity)	Tropical region	RMSE (μmol/L)	1.01	–
		MAE (μmol/L)	0.73	–
	Subtropical region	RMSE (μmol/L)	0.58	–
		MAE (μmol/L)	0.46	–
Experiment 2 (with salinity)	Tropical region	RMSE (μmol/L)	0.92	9%
		MAE (μmol/L)	0.72	1.4%
	Subtropical region	RMSE (μmol/L)	0.48	17.2%
		MAE (μmol/L)	0.38	17.4%

This circumstance reminds us that salinity should be carefully considered when predicting nitrate concentrations in middle and high latitudes.

4.2. *Vertical distribution of nitrate estimated by WOA18 data*

To verify the generalization ability of our trained DNN model, both temperature and salinity data of WOA18 were used to estimate nitrate concentration. The 137°E section is selected because of the significant meridional variations of nitrate which have been reproduced by our trained model (Fig. 8d–f).

The NSE, RMSE, and MAE of nitrate concentration estimated using WOA18 temperature and salinity are 0.96, 1.99 μmol/L, and 1.57 μmol/L, respectively. The value of NSE was lower than that obtained using JMA data. Overall, the trained model can reproduce the distribution of nitrate along the 137°E section (Fig. 9a and b). The differences are more obvious in the nitrate-cline, especially in 4°N and 31°N (Fig. 9c). The nitrate concentration is underestimated. We checked the temperature difference between WOA18 and JMA data. The temperature data of WOA and JMA show obvious differences in some areas, such as the area around 4°N and 31°N (Fig. 10). This is similar to the nitrate difference (Fig. 9c). As shown in Fig. 10, the JMA temperature is lower than WOA18 temperature in the area around 4°N and 31°N. According to the inverse temperature-nitrate relation (Kudela and Chavez, 2000; Strickland et al., 1970; Traganza et al., 1983), it is clear that why the nitrate concentration obtained is underestimated.

5. Conclusions

In this study, a DNN model is developed and applied to estimate nitrate concentrations in the upper NPO. The results indicated that the designed DNN model can estimate nitrate concentration accurately in both tropical region (NSE = 0.99, RMSE = 0.92 μmol/L, MAE = 0.48 μmol/L) and subtropical region (NSE = 0.99, RMSE = 0.72 μmol/L, MAE = 0.38 μmol/L). The DNN model performs well in both winter and summer (RMSE less than 1.04 μmol/L), indicating that the DNN model has a good seasonal applicability for the nitrate estimation in NPO. In addition, compared with observations along a zonal section (9°N section) and a meridional section (137°E section), the DNN model also does well in reproducing the zonal and meridional distribution of nitrate. The

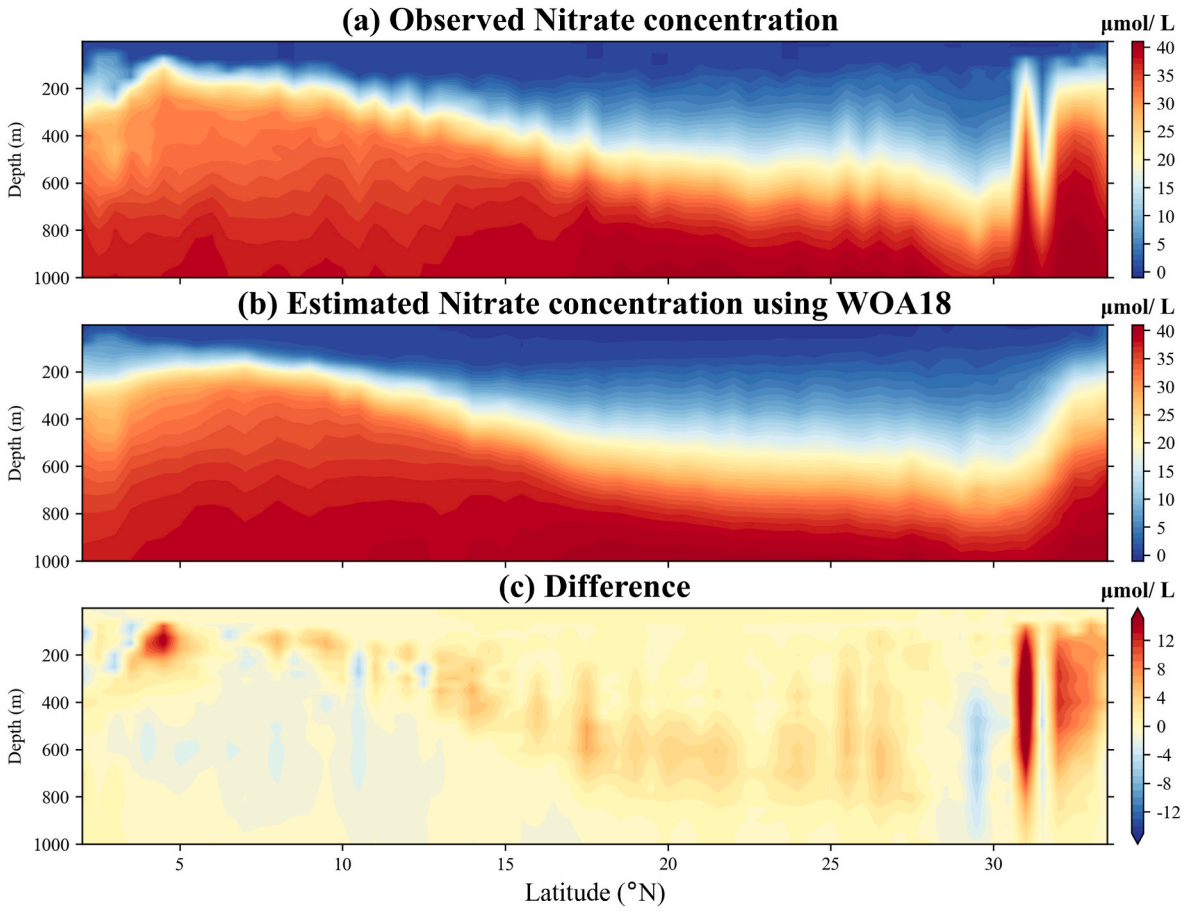

Fig. 9. Vertical distribution of nitrate concentrations along the 137°E section derived from (a) observation data and (b) the model estimates based on WOA18 data. (c) The difference between (a) and (b).

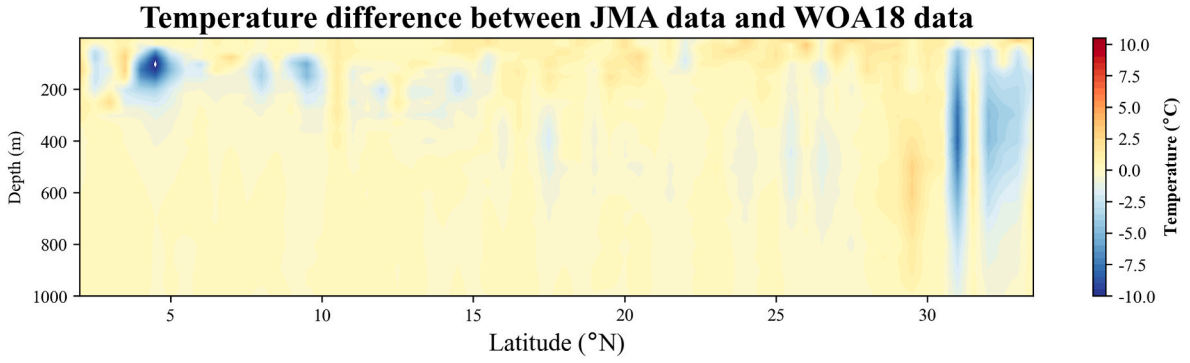

Fig. 10. Difference between JMA and WOA18 temperature (JMA minus WOA18) along the 137°E section.

sensitivity experiments demonstrated that inputting salinity could significantly increase the accuracy of estimation, especially in the subtropical region. By inputting the temperature and salinity profiles from WOA18 data into our trained DNN model, we demonstrate that our model has a good generalization ability. The vertical distribution of nitrate along the 137°E section estimated from WOA18 data agrees well with the observed distribution.

As a data-dependence method, the model performance was highly dependent on data quality. It means that in some circumstances, the model performance may be significantly weakened by the scarcity of data. For example, due to the lack of data in spring and autumn, we are unable to train a model which can depict the distribution in these two seasons. A future improvement of our model involves employing additional input variables such as chlorophyll (Goes et al., 1999, 2000) and dissolved oxygen (Sauzède et al., 2017) that potentially affect nitrate concentrations. Once the nitrate has been accurately estimated, it can be used for practical applications, such as new production estimates and understanding the global carbon cycle.

Author contributions

Conceptualization, Z.H.X., X.G.; Methodology, W.L.X., X.G.; Formal analysis: W.L.X., P.W.Z., Z.J.H, J.Y., X.Z.Z; Writing - Original draft, W.L.X., P.W.Z., Z.J.H, J.Y.; Writing - Reviewing & Editing, Z.H.X., X.G., W.L.X., P.W.Z., Z.J.H, J.Y., and X.Y.G..

Declaration of competing interest

The authors declare that they have no known competing financial interests or personal relationships that could have appeared to influence the work reported in this paper.

Data availability

The datasets for this study are publicly available. The in-situ data are provided by the Japan Meteorological Agency (JMA, https:/www.data.jma.go.jp). This monthly dataset of World Ocean Atlas (2018) can be downloaded from the Asia Pacific Data Research Center (ARDRC, http://apdrc.soest.hawaii.edu/as/v6/search).

Acknowledgments

This study was jointly supported by the Strategic Priority Research Program of the Chinese Academy of Sciences and the National Nature Science Foundation of China-Shandong Joint Fund (XDA22050202, U1906215, XDB42000000), National Natural Science Foundation of China (92058202), the Scientific and Technological Innovation Project financially supported by Laoshan Laboratory (LSKJ202202502), Key Deployment Project of Center for Ocean Mega Research of Science, Chinese Academy of Sciences (COMS2020Q07), the project jointly funded by the CAS and CSIRO (133244KYSB20190031).

References

Bittig, H.C., Steinhoff, T., Claustre, H., Fiedler, B., Williams, N.L., Sauzède, R., Gattuso, J. P., 2018. An alternative to static climatologies: robust estimation of open ocean CO_2 variables and nutrient concentrations from T, S, and O_2 data using Bayesian neural networks. Front. Mar. Sci. 5, 328. https://doi.org/10.3389/fmars.2018.00328.

Chen, J., Gong, X., Guo, X., Xing, X., Lu, K., Gao, H., Gong, X., 2022. Improved perceptron of subsurface chlorophyll maxima by a deep neural network: a case study with BGC-argo float data in the northwestern Pacific Ocean. Rem. Sens. 14, 632. https://doi.org/10.3390/rs14030632.

Chen, Z., Sun, J., Chen, D., Wang, S., Yu, H., Chen, H., Wang, M., 2021. Effects of ocean currents in the western Pacific Ocean on net-phytoplankton community compositions. Diversity 13 (9), 428. https://doi.org/10.3390/d13090428.

Dong, C., Xu, G., Han, G., Bethel, B.J., Xie, W., Zhou, S., 2022. Recent developments in artificial intelligence in oceanography. Ocean-Land-Atmosphere Research. https://doi.org/10.34133/2022/9870950, 2022.

Feng, M., McPhaden, M.J., Lee, T., 2010. Decadal variability of the Pacific subtropical cells and their influence on the southeast Indian Ocean. Geophys. Res. Lett. 37 (9) https://doi.org/10.1029/2010GL042796.

Fourrier, M., Coppola, L., Claustre, H., D' Ortenzio, F., Sauzède, R., Gattuso, J.P., 2020. A regional neural network approach to estimate water-column nutrient concentrations and carbonate system variables in the Mediterranean Sea: canyon-med. Front. Mar. Sci. 7, 620. https://doi.org/10.3389/fmars.2020.00620.

Friedrich, T., Oschlies, A., 2009. Neural network-based estimates of North Atlantic surface pCO2 from satellite data: a methodological study. J. Geophys. Res.: Oceans 114. https://doi.org/10.1029/2007JC004646.

Garcia, H.E., Boyer, T.P., Baranova, O.K., Locarnini, R.A., Mishonov, A.V., Grodsky, A.E., Zweng, M.M., 2019. World ocean atlas 2018: Product documentation. A. Mishonov, Technical Editor.

Garside, C., Garside, J.C., 1995. Euphotic-zone nutrient algorithms for the NABE and EqPac study sites. Deep Sea Res. Part II Top. Stud. Oceanogr. 42, 335–347. https://doi.org/10.1016/0967-0645(95)00026-M.

George, J.V., Nuncio, M., Chacko, R., Anilkumar, N., Noronha, S.B., Patil, S.M., 2013. Role of physical processes in chlorophyll distribution in the western tropical Indian Ocean. J. Mar. Syst. 113, 1–12.

Gevrey, M., Dimopoulos, I., Lek, S., 2003. Review and comparison of methods to study the contribution of variables in artificial neural network models. Ecol. Model. 160 (3), 249–264. https://doi.org/10.1016/S0304-3800(02)00257-0.

Goes, J.I., Saino, T., Oaku, H., Jiang, D.L., 1999. A method for estimating sea surface nitrate concentrations from remotely sensed SST and chlorophyll aa case study for the north Pacific Ocean using OCTS/ADEOS data. IEEE Trans. Geosci. Rem. Sens. 37, 1633–1644. https://doi.org/10.1109/36.763279.

Goes, J.I., Saino, T., Oaku, H., Ishizaka, J., Wong, C.S., Nojiri, Y., 2000. Basin scale estimates of sea surface nitrate and new production from remotely sensed sea surface temperature and chlorophyll. Geophys. Res. Lett. 27, 1263–1266. https://doi.org/10.1029/1999GL002353.

Guo, L., Chai, F., Xiu, P., Xue, H., Rao, S., Liu, Y., Chavez, F.P., 2014. Seasonal dynamics of physical and biological processes in the central California Current System: a modeling study. Ocean Dynam. 64 (8), 1137–1152. https://doi.org/10.1007/s10236-014-0721-x.

Huang, Y., Fan, D., Liu, D., Song, L., Ji, D., Hui, E., 2016. Nutrient estimation by HJ-1 satellite imagery of xiangxi bay, three gorges reservoir, China. Environ. Earth Sci. 75, 1–13. https://doi.org/10.3882/j.issn.1674-2370.2014.01.008.

Jamet, C., Loisel, H., Dessailly, D., 2012. Retrieval of the spectral diffuse attenuation coefficient Kd (λ) in open and coastal ocean waters using a neural network inversion. J. Geophys. Res.: Oceans 117. https://doi.org/10.1029/2012JC008076.

Kanda, J., 2008. Vertical profiles of nitrate uptake obtained from in situ 15N incubation experiments in the western North Pacific. J. Mar. Syst. 71 (1–2), 63–78. https://doi.org/10.1016/j.jmarsys.2007.05.005.

Khumprom, P., Yodo, N., 2019. A data-driven predictive prognostic model for lithium-ion batteries based on a deep learning algorithm. Energies 12 (4), 660. https://doi.org/10.3390/en12040660.

Kim, N., Ha, K.J., Park, N.W., Cho, J., Hong, S., Lee, Y.W., 2019. A comparison between major artificial intelligence models for crop yield prediction: case study of the midwestern United States, 2006-2015. ISPRS Int. J. Geo-Inf. 8 (5), 240. https://doi.org/10.3390/ijgi8050240.

Kim, T.W., Lee, K., Najjar, R.G., Jeong, H.D., Jeong, H.J., 2011. Increasing N abundance in the northwestern Pacific Ocean due to atmospheric nitrogen deposition. Science 334, 505–509. https://doi.org/10.1126/science.1206583.

Kudela, R.M., Chavez, F.P., 2000. Modeling the impact of the 1992 el niño on new production in monterey bay, California. Deep Sea Res. Part II Top. Stud. Oceanogr. 47, 1055–1076. https://doi.org/10.1016/S0967-0645(99)00136-8.

Kudela, R.M., Dugdale, R.C., 1996. Estimation of new production from remotely-sensed data in a coastal upwelling regime. Adv. Space Res. 18, 91–97. https://doi.org/10.1016/0273-1177(95)00952-3.

Lewis, M.R., Hebert, D., Harrison, W.G., Platt, T., Oakey, N.S., 1986. Vertical nitrate fluxes in the oligotrophic ocean. Science 234 (4778), 870–873. https://doi.org/10.1126/science.234.4778.870.

Li, X., Zhou, Y., Wang, F., 2022. Advanced information mining from ocean remote sensing imagery with deep learning. Journal of Remote Sensing. https://doi.org/10.34133/2022/9849645.

Li, Y., Wang, F., 2013. Thermohaline intrusions in the thermocline of the western tropical Pacific Ocean. Acta Oceanol. Sin. 32, 47–56. https://doi.org/10.1007/s13131-013-0331-3.

Li, Z., Cai, Z., Liu, Z., Wang, X., Hu, J., 2022. A novel identification method for unrevealed mesoscale eddies with transient and weak features-Capricorn Eddies as an example. Rem. Sens. Environ. 274, 112981 https://doi.org/10.1016/j.rse.2022.112981.

Long, Y., Guo, X., Zhu, X.H., Li, Z., 2022. Nutrient streams in the North Pacific. Prog. Oceanogr. 202, 102756 https://doi.org/10.1016/j.pocean.2022.102756.

Lou, R., Wang, W., Li, X., Zheng, Y., Lv, Z., 2021. Prediction of ocean wave height suitable for ship autopilot. IEEE Trans. Intell. Transport. Syst. https://doi.org/10.1109/TITS.2021.3067040.

Lu, K., Wang, W., Gao, S., Pang, X., 2020. Application of multi-layer forward neural network based piecewise linear regressionin simulation of steam turbine valve flow curve. In: IOP Conference Series: Earth and Environmental Science. IOP Publishing. https://doi.org/10.1088/1755-1315/512/1/012170.

Lukas, R., Lindstrom, E., 1991. The mixed layer of the western equatorial Pacific Ocean. J. Geophys. Res.: Oceans 96 (S01), 3343–3357. https://doi.org/10.1029/90JC01951.

May, R., Dandy, G., Maier, H., 2011. Review of input variable selection methods for artificial neural networks. Artificial neural networks-methodological advances and biomedical applications 10 (1), 19–45.

Ma, X., Sun, C., 2015. Water mass characteristics in the western North Pacific based on a streamfunction projection. Sci. China Earth Sci. 58, 2067–2077. https://doi.org/10.1007/s11430-015-5100-z.

Morin, P.M.V.M., Wafar, M.V.M., Le Corre, P., 1993. Estimation of nitrate flux in a tidal front from satellite-derived temperature data. J. Geophys. Res.: Oceans 98, 4689–4695. https://doi.org/10.1029/92JC02445.

Mustapha, Z.B., Alvain, S., Jamet, C., Loisel, H., Dessailly, D., 2014. Automatic classification of water-leaving radiance anomalies from global SeaWiFS imagery: application to the detection of phytoplankton groups in open ocean waters. Rem. Sens. Environ. 146, 97–112. https://doi.org/10.1016/j.rse.2013.08.046.

Rafter, P.A., Sigman, D.M., Charles, C.D., Kaiser, J., Haug, G.H., 2012. Subsurface tropical Pacific nitrogen isotopic composition of nitrate: biogeochemical signals and their transport. Global Biogeochem. Cycles 26 (1). https://doi.org/10.1029/2010GB003979.

Reichstein, M., Camps-Valls, G., Stevens, B., Jung, M., Denzler, J., Carvalhais, N., 2019. Deep learning and process understanding for data-driven Earth system science. Nature 566, 195–204. https://doi.org/10.1038/s41586-019-0912-1.

Ren, L., Riser, S.C., 2010. Observations of decadal time scale salinity changes in the subtropical thermocline of the North Pacific Ocean. Deep Sea Res. Part II Top. Stud. Oceanogr. 57 (13–14), 1161–1170. https://doi.org/10.1016/j.dsr2.2009.12.005.

Sammartino, M., Marullo, S., Santoleri, R., Scardi, M., 2018. Modelling the vertical distribution of phytoplankton biomass in the Mediterranean Sea from satellite data: a neural network approach. Rem. Sens. 10, 1666. https://doi.org/10.3390/rs10101666.

Sarangi, R.K., 2011. Remote-sensing-based estimation of surface nitrate and its variability in the southern peninsular Indian waters. International Journal of Oceanography. https://doi.org/10.1155/2011/172731, 2011.

Sarmiento, J.L., Gruber, N., Brzezinski, M.A., Dunne, J.P., 2004. High-latitude controls of thermocline nutrients and low latitude biological productivity. Nature 427, 56–60. https://doi.org/10.1038/nature10605.

Sauzède, R., Bittig, H.C., Claustre, H., Pasqueron de Fommervault, O., Gattuso, J.P., Legendre, L., Johnson, K.S., 2017. Estimates of water-column nutrient concentrations and carbonate system parameters in the global ocean: a novel

approach based on neural networks. Front. Mar. Sci. 4, 128. https://doi.org/10.3389/fmars.2017.00128.
Sharma, S., Sharma, S., Athaiya, A., 2017. Activation functions in neural networks. Data Sci. 6 (12), 310–316. https://doi.org/10.33564/ijeast.2020.v04i12.054.
Silió-Calzada, A., Bricaud, A., Uitz, J., Gentili, B., 2008. Estimation of new primary production in the Benguela upwelling area, using ENVISAT satellite data and a model dependent on the phytoplankton community size structure. J. Geophys. Res.: Oceans 113. https://doi.org/10.1029/2007JC004588.
Steinhoff, T., Friedrich, T., Hartman, S.E., Oschlies, A., Wallace, D.W., Körtzinger, A., 2010. Estimating mixed layer nitrate in the North Atlantic ocean. Biogeosciences 7 (3), 795–807. https://doi.org/10.5194/bg-7-795-2010.
Strickland, J.D.H., Solorzano, L., Eppley, R.W., 1970. General Introduction, Hydrography, and Chemistry. Calif Univ Scripps Inst Oceanogr Bull.
Sun, C., Rienecker, M.M., Rosati, A., Harrison, M., Wittenberg, A., Keppenne, C.L., Kovach, R.M., 2007. Comparison and sensitivity of ODASI ocean analyses in the tropical Pacific. Mon. Weather Rev. 135 (6), 2242–2264. https://doi.org/10.1175/MWR3405.1.
Sun, Y., Yao, X., Bi, X., Huang, X., Zhao, X., Qiao, B., 2021. Time-series graph network for sea surface temperature prediction. Big Data Research 25, 100237. https://doi.org/10.1016/j.bdr.2021.100237.
Talley, L.D., Feely, R.A., Sloyan, B.M., Wanninkhof, R., Baringer, M.O., Bullister, J.L., Zhang, J.Z., 2016. Changes in ocean heat, carbon content, and ventilation: a review of the first decade of GO-SHIP global repeat hydrography. Ann. Rev. Mar. Sci 8 (1). https://doi.org/10.1146/annurev-marine-052915-100829.
Traganza, E.D., Silva, V.M., Austin, D.M., Hanson, W.L., Bronsink, S.H., 1983. Nutrient mapping and recurrence of coastal upwelling centers by satellite remote sensing: its implication to primary production and the sediment record. In: Coastal Upwelling its Sediment Record. Springer, Boston, MA, pp. 61–83. https://doi.org/10.1007/978-1-4615-6651-9_4.
Tsunogai, S., 2002. The western North Pacific playing a key role in global biogeochemical fluxes. J. Oceanogr. 58 (2), 245–257. https://doi.org/10.1023/A:1015805607724.
Uddin, M.G., Nash, S., Diganta, M.T.M., Rahman, A., Olbert, A.I., 2022. Robust machine learning algorithms for predicting coastal water quality index. J. Environ. Manag. 321, 115923 https://doi.org/10.1016/j.jenvman. 2022. 115923.
Wang, D., Cui, Q., Gong, F., Wang, L., He, X., Bai, Y., 2018. Satellite retrieval of surface water nutrients in the coastal regions of the East China Sea. Rem. Sens. 10 (12), 1896. https://doi.org/10.3390/rs10121896.
Webb, P., 2021. Introduction to oceanography. Roger Williams University 5 (6).
Xiu, P., Chai, F., 2011. Modeled biogeochemical responses to mesoscale eddies in the South China Sea. J. Geophys. Res.: Oceans 116 (C10). https://doi.org/10.1029/2010JC006800.
Yang, W., Wei, H., Zhao, L., Zhang, J., 2020. Turbulence and vertical nitrate flux adjacent to the Changjiang Estuary during fall. J. Mar. Syst. 212, 103427 https://doi.org/10.1016/j.jmarsys.2020.103427.
Yasunaka, S., Nojiri, Y., Nakaoka, S.I., Ono, T., Whitney, F.A., Telszewski, M., 2014. Mapping of sea surface nutrients in the North Pacific: basin-wide distribution and seasonal to interannual variability. J. Geophys. Res.: Oceans 119 (11), 7756–7771. https://doi.org/10.1002/2014JC010318.
Yu, X., McPhaden, M.J., 1999. Seasonal variability in the equatorial Pacific. J. Phys. Oceanogr. 29 (5), 925–947. https://doi.org/10.1175/1520-0485(1999)029<0925:SVITEP>2.0.CO;2.
Zare, A., Bayat, V., Daneshkare, A., 2011. Forecasting nitrate concentration in groundwater using artificial neural network and linear regression models. Int. Agrophys. 25 (2).
Zhang, Q., Cai, R., Qi, Q., Zheng, D., 2007. Spatial and temporal variations of temperature and salinity field along 137°E section in northwestern Pacific Ocean. J. Oceanogr. Taiwan Strait 26 (4), 453. https://doi.org/10.3969/j.issn.1000-8160.2007.04.001.
Zhang, X., Li, X., 2022. Satellite data-driven and knowledge-informed machine learning model for estimating global internal solitary wave speed. Rem. Sens. Environ. 283, 113328 https://doi.org/10.1016/j.rse.2022.113328.
Zhang, Y., Pulliainen, J., Koponen, S., Hallikainen, M., 2002. Application of an empirical neural network to surface water quality estimation in the Gulf of Finland using combined optical data and microwave data. Rem. Sens. Environ. 81 (2–3), 327–336. https://doi.org/10.1016/S0034-4257(02)00009-3.
Zhou, J., Luo, X., Xiao, J., Wei, H., Zhao, W., Zheng, Z., 2021. Modeling the seasonal and interannual variations in nitrate flux through Bering Strait. J. Mar. Syst. 218, 103527 https://doi.org/10.1016/j.jmarsys.2021.103527.